Interstitial lithium doping in SrTiO3

Kuganathan, K., Baiutti, F., Morata, A., Tarancón, A. & Chroneos, A.

DOI 10.1063/5.0059306
ESSN 2158-3226

Publisher: American Institute of Physics

Interstitial lithium doping in $SrTiO_3$

Cite as: AIP Advances 11, 075029 (2021); doi: 10.1063/5.0059306
Submitted: 8 June 2021 • Accepted: 30 June 2021 •
Published Online: 26 July 2021

Navaratnarajah Kuganathan,[1,2,a)] Federico Baiutti,[3] Alex Morata,[3] Albert Tarancon,[3,4] and Alexander Chroneos[1,2]

AFFILIATIONS

[1] Faculty of Engineering, Environment and Computing, Coventry University, Priory Street, Coventry CV1 5FB, United Kingdom
[2] Department of Materials, Imperial College London, London SW7 2AZ, United Kingdom
[3] Catalonia Institute for Energy Research (IREC), Jardins de Les Dones de Negre 1, 08930 Sant Adria' Besos, Barcelona, Spain
[4] ICREA, 23 Passeig Lluís Companys, Barcelona 08010, Spain

[a)] **Author to whom correspondence should be addressed:** n.kuganathan@imperial.ac.uk

ABSTRACT

Strontium titanate ($SrTiO_3$) has received much attention due to its wide range of potential applications, including in electrochemical devices such as solid oxide fuel cells and capacitors. The stability and safety features of $SrTiO_3$ led to the development of promising electrodes for Li-ion batteries. Here, we use density functional theory simulations to examine the incorporation of lithium from its gas-phase and bulk forms. The results show that a single Li atom is thermodynamically stable in bulk $SrTiO_3$ with respect to its gas-phase and slightly unfavorable compared to its bulk. Multiple Li incorporation up to six is also considered, and the incorporation is exoergic with respect to both gas-phase and bulk forms. Charge analysis confirmed the presence of Li^+ ions in the lattice. Li incorporation turns the insulating nature of $SrTiO_3$ into metallic and non-magnetic into magnetic. Lithium incorporation facilitates the formation of Sr, Ti, and O vacancies. The loss of Li_2O is exoergic, suggesting that oxygen vacancy mediated self-diffusion will be promoted.

I. INTRODUCTION

There is a global search for renewable energy resources due to the growing energy demand for large-scale applications such as electric vehicles and grid-scale energy storage systems. Lithium ion batteries (LIBs) are emerging as a potential renewable energy source and widely used as a primary power source in consumer electronics.[1–4] However, there is a necessity to develop new materials to optimize the performance of LIBs, especially for hybrid vehicles.

Transition metal oxide perovskites have gained widespread recognition as anodes for its utility in electrochemical energy storage devices, including LIBs, owing to their low cost, environmentally benign nature, non-toxicity, and cyclic performance.[5–8] Furthermore, perovskite oxide hosts have the ability to overcome the volume expansion during lithium intercalation.[6] In a recent electrochemical study, perovskite-type $CaMnO_3$ has been shown to be a candidate anode material for LIBs with promising specific capacity, rate performance, and cyclic stability.[9] Another experimental study by Yan *et al.*[6] showed that entropy stabilized aliovalent doped-perovskite titanates provide excellent cycle and rate performance. Although there is a limited number of perovskite oxide based host structures identified, the search for other members in this family of oxides continues.

$SrTiO_3$ (STO) has appropriate properties (semiconductor, ferroelectric, ion conductor, and catalytic) suitable for practical applications such as gas sensors, fuel cells, and thermoelectrics.[10–15] The suitability of this material for those applications can be attributed to its stability over a wide temperature range, and this is partly due to the corner sharing strong TiO_6 octahedral units. The modification of this material via doping of a variety of aliovalent dopants has been comprehensively studied in order to maximize its utility in catalysis, electronics, and thermoelectrics.[16–19] Johnson and Prieto[20] had experimentally shown the impact of heavy hydrogen doping on the resistivity and electronic properties of STO. In their study, doping had dramatically reduced the resistivity, and the resultant thinfilm exhibited a metallic nature. Nevertheless, despite the demonstrated stability and the environmental friendliness of STO, the exploration of this material in the Li-ion field is limited.[22,23] The main reason could be found in its low electronic conductivity, which can be a limitation for electrode performance. Some strategies are, however, possible to overcome this issue, similar to the one adopted by Karaphun *et al.*,[22] implementing nanoscale Pt modules to facilitate

the insertion of charges to and from the STO surface to the binder. The as-prepared non-lithiated conducting metals intercalated with STO nanoparticles to test its efficacy as an anode materal for LIBs, showing a reasonable capacity of 135 mA h g^{-1} (85% of the theoretical) when cycling at low rates.

These results demonstrate the feasibility of including STO in the list of safe and stable Ti-based Li-ion anodes. However, although the experimental reports provide the electrochemical performance of these materials, there is no report available on the structures of intercalated Li, the nature of incorporation, structural stability, and electronic structures of resultant incorporated complexes.

Bulk STO has a large number of octahedral interstitial sites that can be accommodated by lithium ions. A reaction between insulating STO and bulk Li is anticipated to produce Li^+ ions and an electron in the lattice simultaneously. This experimental strategy can make STO electronically conductive together with the presence of Li^+ ions.

In this study, we used density functional theory (DFT) to calculate the structure of Li atoms (up to 6) incorporated into STO from its bulk and isolated gas forms. The current methodology enabled us to calculate the incorporation energies, charges on the incorporated Li atoms, the magnetic moments of the resultant complexes, and the electronic structures of both pristine STO and Li-incorporated structures.

II. COMPUTATIONAL METHODS

All calculations were performed using a DFT code VASP (Vienna *ab initio* Simulation Package) code,[24] which solves standard Kohn–Sham equations using plane wave basis sets and projected augmented wave (PAW) pseudopotentials.[25] A plane wave basis set with a cut-off of 500 eV was used. For bulk $SrTiO_3$, an 8 × 8 × 8 Monkhorst–Pack[26] *k*-point mesh was used. All defect calculations were performed using a 3 × 3 × 3 supercell containing 135 atoms. For defect modeling, we used a 2 × 2 × 2 Monkhorst–Pack *k*-point mesh. The exchange-correlation energy was modeled using the generalized gradient approximation (GGA) scheme as described by Perdew, Burke, and Ernzerhof (PBE).[27] The conjugate gradient algorithm[28] was used to perform full geometry optimization in which both atom positions and lattice constants were relaxed simultaneously. In all relaxed configurations, forces on the atoms were less than 0.001 eV/Å. In order to describe the behavior of localized Ti 3*d* states, we included orbital dependent, Coulomb potential (Hubbard U) and the exchange parameter J within the DFT+U calculations, as formulated by Akbar *et al.*[29] We applied values of U = 5.80 eV and J = 0.00 eV to the localized 3*d* states of Ti as reported in a previous study.[30]

Incorporation energies of Li atoms were calculated using the following equation:

$$E_{inc} = \frac{E_{xLi:STO} - E_{STO} - xE_{Li}}{x}, \quad (1)$$

where $E_{xLi:STO}$ is the total energy of x number of Li atoms incorporated into a 3 × 3 × 3 STO supercell, E_{STO} is the total energy of a 3 × 3 × 3 supercell, and E_{Li} is the energy of an isolated gas phase Li atom or atomic Li in its bulk.

III. RESULTS AND DISCUSSION

A. Crystal structure of $SrTiO_3$

Cubic perovskite phase $SrTiO_3$ crystallizes in the space group $Pm\bar{3}m$ (no. 221).[31] Its experimental lattice parameters are reported to be a = b = c = 3.9051 Å and $\alpha = \beta = \gamma = 90°$.[31] The strontium ions form complexes (coordination number = 12) with adjacent oxygen atoms and occupy the body centered positions of the crystal. The titanium ions form corner sharing TiO_6 octahedral units, and they are connected to form a three dimensional network as shown in Fig. 1(a). In order to validate the pseudopotentials and basis sets used for Sr, Ti, and O, we optimized both ion positions and lattice constants of STO to obtain equilibrium lattice constants. There is good agreement between the calculated and experimental lattice constants, showing the efficacy of the potential parameters (see Table I). To obtain a good band structure, we introduced a Hubbard U parameter for *d*-states of Ti and compared the electronic structures of bulk STO calculated with and without U parameters. The calculated lattice parameters using the Hubbard U parameter are slightly larger than that calculated without U. However, the DFT+U approach provided a better bandgap value than that calculated using DFT [see Figs. 1(b) and 1(c)]. Thus, we opted to use the DFT+U method in the defect calculations.

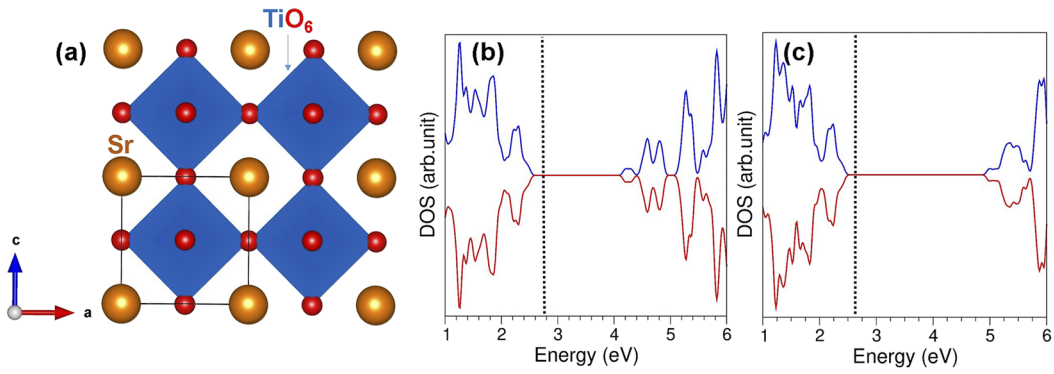

FIG. 1. (a) Crystal structure of cubic perovskite STO (space group $Pm\bar{3}m$) and (b) and (c) calculated DOS plots of STO with and without Hubbard parameter U, respectively.

TABLE I. Calculated lattice parameters and bandgap values together with their corresponding experimental values.

	Calculated			|Δ| (%)	
Parameter	DFT	DFT+U	Expt.[31]	DFT	DFT+U
a = b = c (Å)	3.931	3.982	3.905	0.67	1.97
α = β = γ (Å)	90.0	90.0	90.0	0.00	0.00
V (Å^3)	60.73	63.15	59.56	1.96	6.02
E_{gap} (eV)	1.50	2.25	3.25	53.85	30.76

The magnetic moment of the relaxed structure is zero, meaning that bulk STO is non-magnetic, in agreement with the experiment[32] and other theoretical studies.[33]

B. Incorporation of a single Li in STO

First, we considered the incorporation of a single Li atom to investigate its stability in bulk STO. Different interstitial positions were considered, and their relaxed structures together with their relative energies are provided in the supplementary material (refer to Fig. S1 and Table S1). The calculated lattice parameters of Li bulk together with the experimental values are provided in the supplementary material (Table S2). The lowest energy structure is shown in Fig. 2(a). Lithium occupies the center of the octahedron formed by four Ti and two Sr atoms. In the distorted LiO_4Sr_2 octahedral unit, the Li–O bond distances and Sr–Li bond distances are calculated to be 1.92 Å (×4) and 2.44 Å (×2), respectively. The longer Sr–Li bond distance is due to the repulsion between the positively charged Sr (+1.58) and Li (+1.00), according the Bader charge analysis.[33] Incorporation energies calculated using a single gas phase Li atom and a Li atom in its bulk as reference states were −1.03 and 0.64 eV, respectively. The negative incorporation energy indicates that the gas phase Li atom is stable inside STO. In contrast, the incorporation energy calculated using the Li atom in its bulk is slightly endothermic. This is due to the extra energy needed to extract a single Li atom from its bulk. A small volume expansion of 0.49% was noted upon Li incorporation.

The calculated total DOS plot [refer to Fig. 2(b)] shows that Li.STO is metallic. This is due to the additional states occupied at the Fermi energy level upon incorporation. A significant Fermi energy shift from 2.62 to 3.90 eV is also noted. Charge density associated with these states are uniformly distributed and localized on the Ti atoms. This can be due to the transfer of an electron from the Li to the Ti atoms.

The magnetic moment of the resultant complex is calculated to be one. This is because of an electron being introduced in the lattice by the Li atom.

C. Incorporation of multiple Li atoms in STO

Next, we considered the incorporation of up to 6 Li atoms in STO. Figure 3 shows the relaxed structures. Here, we considered multiple Li atoms at different positions in the lattice. The lowest energy structures are reported here. In the supplementary material, we provide all configurations considered and their relative energies (see Figs. S2–S6 and Tables S3–S7). In all cases, Li occupies the octahedral sites forming four shorter Li–O bonds and two longer Li–Sr

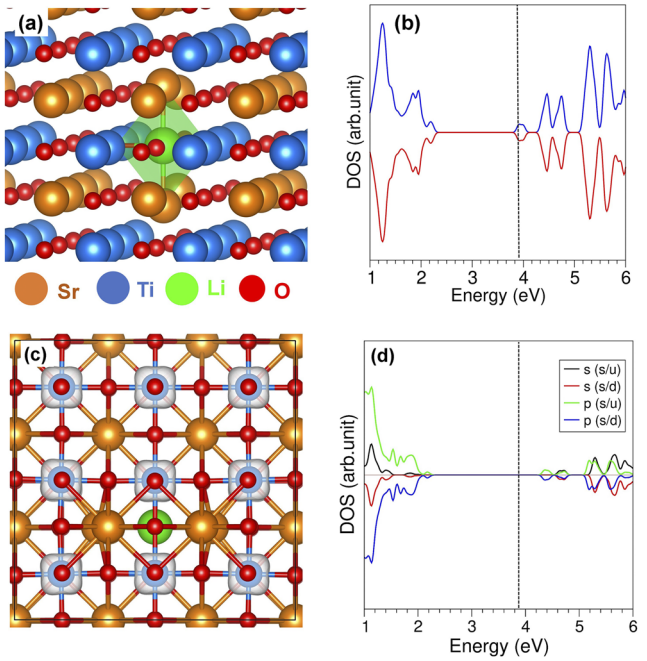

FIG. 2. (a) Relaxed structure of a single Li atom incorporated in STO, (b) the total DOS, (c) the charge density plot associated with the states that appear at the Fermi level, and (d) the atomic DOS plot of Li.

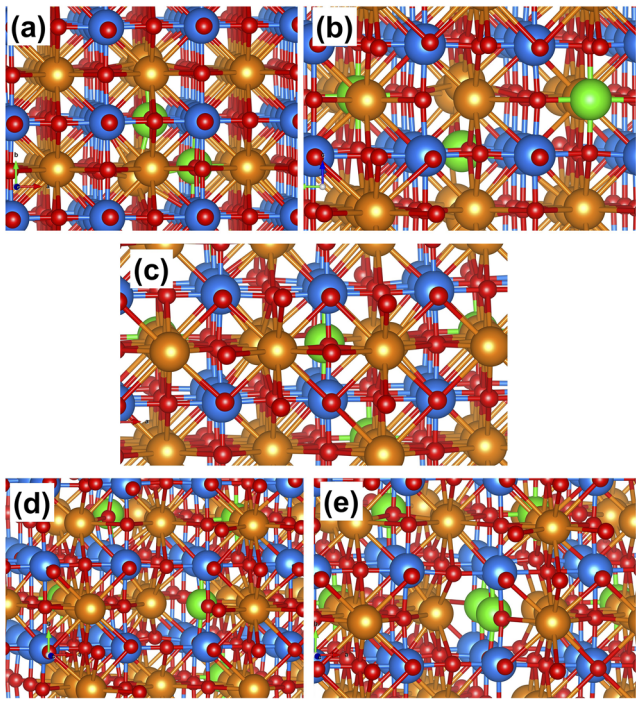

FIG. 3. Relaxed structures of (a) 2Li.STO, (b) 3Li.STO, (c) 4Li.STO, (d) 5Li.STO, and (e) 6Li.STO.

TABLE II. Incorporation energies, Bader charges on the incorporated Li atoms, bond distances, volume changes, and magnetic moments of the incorporated complexes.

System	Incorporation energy (eV)	Bader charges on Li (|e|)	Li–O (Å)	Li–Sr (Å)	Volume change (%)	Magnetic moment (μ)
2Li.STO	−1.86 (−0.19)	+1.00 (×2)	1.91–1.94	2.48–2.52	1.48	2.00
3Li.STO	−1.85 (−0.18)	+1.00 (×3)	1.93–1.95	2.48–2.50	2.12	3.00
4Li.STO	−1.89 (−0.22)	+1.00 (×4)	1.92–1.95	2.46–2.50	2.91	4.00
5Li.STO	−1.95 (−0.28)	+1.00 (×5)	1.91–1.95	2.46–2.50	3.52	5.00
6Li.STO	−1.96 (−0.29)	+1.00 (×6)	1.92–1.98	2.48–2.55	4.23	6.00

bonds (see Table II). In all cases, incorporation energies are exothermic with respect to bulk Li and the gas phase Li atom, suggesting that Li atoms are more stable in the octahedral interstitial sites. The strong incorporation with respect to the gaseous Li atom as a reference state is due to the higher stability of the Li atom in the bulk than its isolated form. Incorporation energies are not significantly affected by the successive encapsulation. The Bader charge analysis shows that in all cases, Li atoms lose their electrons to form Li^+ ions. This is further confirmed by the shorter Li–O and longer Li–Sr bond distances. The formation of Li^+ ions reflects in the longer Li–Sr bond distances due to cation repulsion. In all cases, bond distances are not altered significantly. Incorporation introduces a linear volume expansion by ~0.7% for every Li. The resultant incorporated complexes are magnetic, and magnetic moment increases by one for each Li. The magnetic nature arises from the loss of one electron from Li.

The calculated DOS plots show that Li-incorporated composites are metallic (see Fig. 4). Band structures for bulk STO and Li-incorporated STO composites are shown in Fig. S7 in the supplementary material. As explained earlier, the metallic nature can be attributed to the electron transfer from Li atoms to the lattice. The Fermi energy changes slightly upon incorporation. The atomic DOS plots calculated for Li show that the states appearing at the Fermi level do not belong to Li. In order to identify those states, we calculated charge density plots associated with the bands at the Fermi level (see Fig. 5). The charge density is mainly localized on the Ti atoms. This indicates that the electrons are mainly gained by the Ti atoms.

D. Formation of vacancies in STO and Li.STO

Next, cation and oxygen vacancy formation energies were calculated in STO and a single Li atom incorporated in STO. Vacancies were created closer to the incorporated Li in order to look at the feasibility of forming vacancies in the presence of Li [see Fig. 6(a)]. Table III reports the defect formation energies. The calculated lattice parameters for the bulk Sr and Ti are reported in Tables S8 and S9 in the supplementary material. Calculations show that defect energies

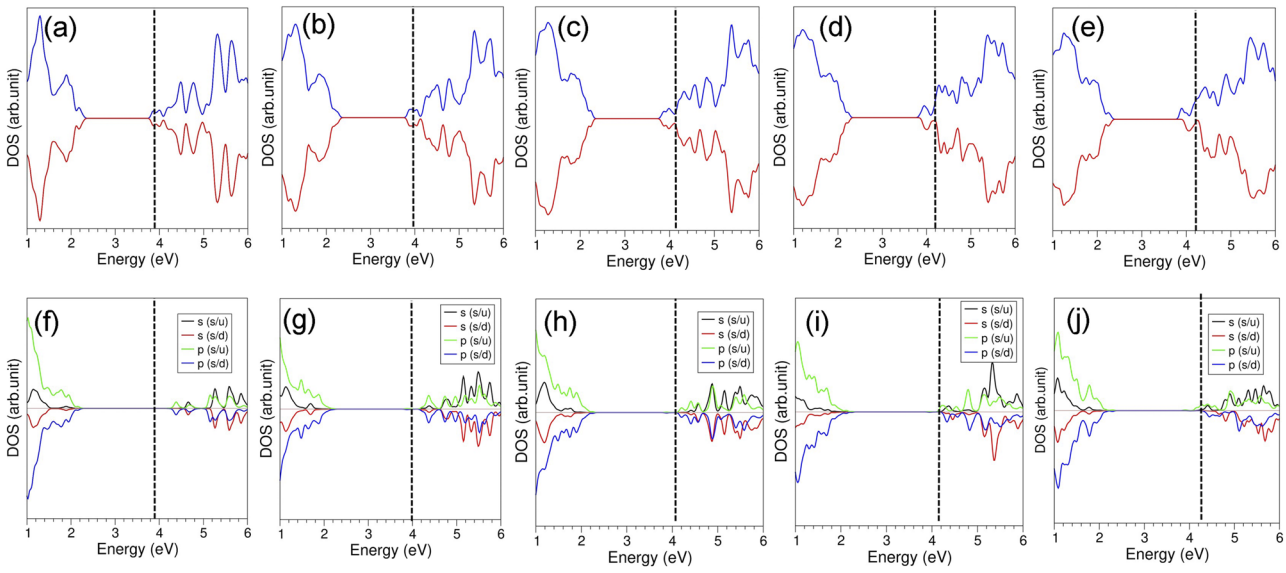

FIG. 4. Total DOS plots of (a) 2Li.STO, (b) 3Li.STO, (c) 4Li.STO, (d) 5Li.STO, and (e) 6Li.STO and (f)–(j) corresponding atomic DOS plots of Li. Black dot vertical lines correspond to the Fermi energy level.

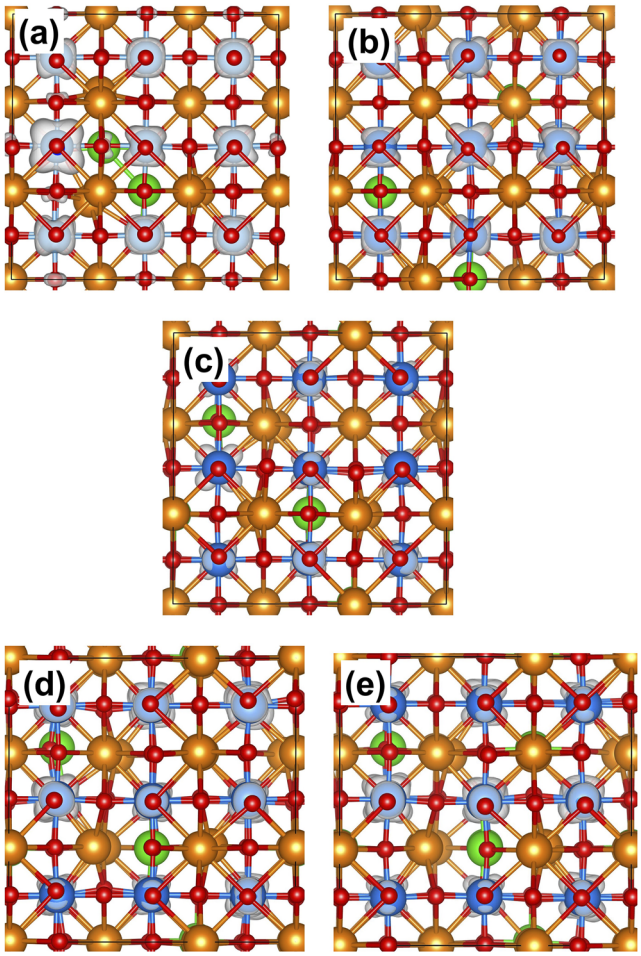

FIG. 5. Charge density plots associated with the states that appear at the Fermi energy level for (a) 2Li.STO, (b) 3Li.STO, (c) 4Li.STO, (d) 5Li.STO, and (e) 6Li.STO.

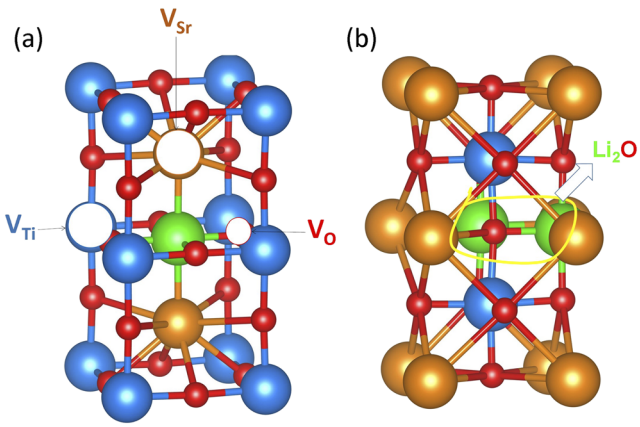

FIG. 6. (a) Vacancies considered in Li.STO and (b) the structure of Li_2O removed from 2Li.STO.

TABLE III. Defect formation energies in pristine STO and Li.STO.

	Defect formation energy (eV)		
System	Sr vacancy	Ti vacancy	O Vacancy
STO	8.64	9.07	5.48
Li.STO	3.72	2.57	4.15

are lowered upon Li incorporation. This is due to the strain introduced by Li in the interstitial positon. In particular, both Sr and Ti are much affected, as evidenced by the relaxed structures and significant formation energy difference (>5 eV). The formation of oxygen vacancy is facilitated by ~1.50 eV upon Li incorporation.

Finally, the removal of Li_2O was considered from 2Li.STO. Figure 6(b) shows the configuration of Li_2O removed from the lattice. The following reaction equation describes the process of removal. The relaxed lattice parameters of bulk Li_2O together with experimental values are given in the supplementary material (see Table S10),

$$2\text{Li.Sr}_{27}\text{Ti}_{27}\text{O}_{81} \rightarrow \text{Li}_2\text{O} + \text{Sr}_{27}\text{Ti}_{27}\text{O}_{80}. \quad (2)$$

An exothermic reaction energy of −1.54 eV indicates that the removal of Li_2O is thermodynamically feasible. The incorporation of Li facilitates the removal of oxygen together with Li forming Li_2O in the lattice.

IV. CONCLUSION

In the present study, the structures and thermodynamical stability of Li atoms incorporated into $SrTiO_3$ were studied using density functional theory. The calculations show that the incorporation of Li atoms is exoergic, suggesting that they are more stable inside $SrTiO_3$ than their isolated forms. Bader charge analysis shows that Li atoms lose their outer electrons to become Li^+ ions. The insulating behavior of $SrTiO_3$ turns metallic upon incorporation, leaving the resultant complex Li^+ rich. Furthermore, the resultant composites formed by Li and $SrTiO_3$ are magnetic. Lithium incorporation facilitates not only the formation of Sr, Ti, and O vacancies but also the formation of Li_2O. These results demonstrate that STO is expected to be a feasible electrode material for Li-ion batteries.

SUPPLEMENTARY MATERIAL

See the supplementary material for the configurations of Li incorporated STO together with their relative energies and band structures.

ACKNOWLEDGMENTS

The research leading to these results has received funding from the European Union's H2020 Programme under Grant Agreement

No. 824072 (HARVESTORE). Computational facilities and support were provided by the High Performance Computing Centre at Imperial College London.

DATA AVAILABILITY

The data that support the findings of this study are available from the corresponding author upon reasonable request.

REFERENCES

[1] M. Li, J. Lu, Z. Chen, and K. Amine, Adv. Mater. **30**, 1800561 (2018).
[2] T. Kim, W. Song, D.-Y. Son, L. K. Ono, and Y. Qi, J. Mater. Chem. A **7**, 2942 (2019).
[3] J. B. Goodenough and K.-S. Park, J. Am. Chem. Soc. **135**, 1167 (2013).
[4] A. Manthiram, ACS Cent. Sci. **3**, 1063 (2017).
[5] R. K. Hona, A. K. Thapa, and F. Ramezanipour, ChemistrySelect **5**, 5706 (2020).
[6] J. Yan, D. Wang, X. Zhang, J. Li, Q. Du, X. Liu, J. Zhang, and X. Qi, J. Mater. Sci. **55**, 6942 (2020).
[7] Z. L. Brown, S. Smith, and M. N. Obrovac, J. Electrochem. Soc. **162**, A15 (2014).
[8] B. L. Phoon, C. W. Lai, J. C. Juan, P. L. Show, and W. H. Chen, Int. J. Energy Res. **43**, 5151 (2019).
[9] L. Chang, J. Li, Z. Le, P. Nie, Y. Guo, H. Wang, T. Xu, and X. Xue, J. Colloid Interface Sci. **584**, 698 (2021).
[10] B. Szafraniak, Ł. Fuśnik, J. Xu, F. Gao, A. Brudnik, and A. Rydosz, Coatings **11**, 185 (2021).
[11] I. Pallecchi, G. Grassano, D. Marré, L. Pellegrino, M. Putti, and A. S. Siri, Appl. Phys. Lett. **78**, 2244 (2001).
[12] A. Atkinson, S. Barnett, R. J. Gorte, J. T. S. Irvine, A. J. McEvoy, M. Mogensen, S. C. Singhal, and J. Vohs, Nat. Mater. **3**, 17 (2004).
[13] S. Tao and J. T. S. Irvine, Chem. Rec. **4**, 83 (2004).
[14] X.-L. Shi, H. Wu, Q. Liu, W. Zhou, S. Lu, Z. Shao, M. Dargusch, and Z.-G. Chen, Nano Energy **78**, 105195 (2020).
[15] J. Sun and D. J. Singh, APL Mater. **4**, 104803 (2016).
[16] T. H. Chiang, H. Lyu, T. Hisatomi, Y. Goto, T. Takata, M. Katayama, T. Minegishi, and K. Domen, ACS Catal. **8**, 2782 (2018).
[17] B. Kiss *et al.*, Appl. Catal., B **206**, 547 (2017).
[18] R. Li, C. Zhang, J. Liu, J. Zhou, and L. Xu, Mater. Res. Express **6**, 102006 (2019).
[19] F. Azough, A. Gholinia, D. T. Alvarez-Ruiz, E. Duran, D. M. Kepaptsoglou, A. S. Eggeman, Q. M. Ramasse, and R. Freer, ACS Appl. Mater. Interfaces **11**, 32833 (2019).
[20] R. Nakayama, M. Maesato, T. Yamamoto, H. Kageyama, T. Terashima, and H. Kitagawa, "Heavy interstitial hydrogen doping into $SrTiO_3$," Chem. Comm. **54**, 12439 (2018).
[21] D. C. Johnson and A. L. Prieto, J. Power Sources **196**, 7736 (2011).
[22] A. Karaphun, S. Kaewmala, N. Meethong, S. Hunpratub, and E. Swatsitang, J. Supercond. Novel Magn. **31**, 1909 (2018).
[23] G. Kresse and J. Furthmüller, Phys. Rev. B **54**, 11169 (1996).
[24] P. E. Blöchl, Phys. Rev. B **50**, 17953 (1994).
[25] H. J. Monkhorst and J. D. Pack, Phys. Rev. B **13**, 5188 (1976).
[26] J. P. Perdew, K. Burke, and M. Ernzerhof, Phys. Rev. Lett. **77**, 3865 (1996).
[27] W. H. Press, S. A. Teukolsky, W. T. Vetterling, and B. P. Flannery, *Numerical Recipes in C: The Art of Scientific Computing*, 2nd ed. (Cambridge University Press, 1992).
[28] S. L. Dudarev, G. A. Botton, S. Y. Savrasov, C. J. Humphreys, and A. P. Sutton, Phys. Rev. B **57**, 1505 (1998).
[29] W. Akbar, T. Liaqat, I. Elahi, M. Zulfiqar, and S. Nazir, J. Magn. Magn. Mater. **500**, 166325 (2020).
[30] R. H. Mitchell, A. R. Chakhmouradian, and P. M. Woodward, Phys. Chem. Miner. **27**, 583 (2000).
[31] J. A. Bert, B. Kalisky, C. Bell, M. Kim, Y. Hikita, H. Y. Hwang, and K. A. Moler, Nat. Phys. **7**, 767 (2011).
[32] P. Sikam, P. Moontragoon, C. Sararat, A. Karaphun, E. Swatsitang, S. Pinitsoontorn, and P. Thongbai, Appl. Surf. Sci. **446**, 92 (2018).
[33] R. F. W. Bader, Theor. Chem. Acc. **105**, 276 (2001).